False vacuum decay in the $(1+1)$-dimensional φ^4 theory

D. Szász-Schagrin[1,2] and G. Takács[1,2,3]

[1]*Department of Theoretical Physics, Institute of Physics, Budapest University of Technology and Economics, H-1111 Budapest, Műegyetem rakpart 3, Hungary*
[2]*BME-MTA Momentum Statistical Field Theory Research Group, Institute of Physics, Budapest University of Technology and Economics, H-1111 Budapest, Műegyetem rakpart 3, Hungary*
[3]*MTA-BME Quantum Dynamics and Correlations Research Group (ELKH), Institute of Physics, Budapest University of Technology and Economics, H-1111 Budapest, Műegyetem rakpart 3, Hungary*

(Received 14 June 2022; accepted 2 July 2022; published 13 July 2022)

The false vacuum is a metastable state that can occur in quantum field theory, and its decay was first studied semiclassically by Coleman. In this work, we consider the $1+1$ dimensional φ^4 theory, which is the simplest model that provides a realization of this problem. We realize the decay as a quantum quench and study the subsequent evolution using a truncated Hamiltonian approach. In the thin wall limit, the decay rate can be described in terms of the mass of the kink interpolating between the vacua in the degenerate limit and the energy density difference between the false and true vacuum once the degeneracy is lifted by a symmetry breaking field, also known as the latent heat. We demonstrate that the numerical simulations agree well with the theoretical prediction for several values of the coupling in a range of the value of the latent heat, apart from a normalization factor, which only depends on the interaction strength.

DOI: 10.1103/PhysRevD.106.025008

I. INTRODUCTION

Tunneling in quantum field theory, also known as the decay of the false vacuum, was first investigated using a semiclassical approach in the groundbreaking work by Coleman [1,2]. Starting with the quantum field stuck in a metastable state called the *false vacuum*, bubbles of the true ground state of the theory (*true vacuum*) nucleate via quantum tunneling. The nucleated bubbles subsequently expand driven by the energy difference between the true and false vacuum, and the released energy (also known as latent heat) also results in a sea of particle excitations filling the newly formed domains of the true vacuum. In the original work by Coleman [1,2], the rate of bubble nucleation was computed in a semiclassical approximation to the path integral using instantons. Recently, it gathered additional attention due to indications of metastability of the Higgs vacuum in the Standard Model [3]. Furthermore, recent advances in experimental technology (e.g., in trapped ultracold atoms) bring direct laboratory study of the phenomenon within reach [4–8].

More generally, the advances in experiments in the past few decades have promoted the out-of-equilibrium dynamics of quantum many-body systems to the forefront of research in condensed matter physics [9–16]. A paradigmatic and experimentally realizable protocol for nonequilibrium dynamics is the so-called quantum quench [17,18], where the system is initially prepared in equilibrium such as a thermal state or a ground state of some Hamiltonian. At the initial time $t=0$, one or more parameters of the theory are suddenly changed, driving the system out of equilibrium subject to subsequent unitary time evolution. The decay of the false vacuum can be naturally implemented as a quantum quench by preparing the system in the false vacuum state as the initial state and studying the resulting time evolution. In the condensed matter context, recently, the phenomenon was also studied in quantum spin chains [19–21].

Nonequilibrium time evolution of nontrivially interacting quantum field theories is rather nontrivial to describe, requiring the use of suitable approximations, both analytic and numerical. For the $1+1$ dimensional φ^4 model, which is the textbook example of a simple interacting quantum field theory, one class of methods is semiclassical approximations such as the mean-field approach [22] or the truncated Wigner approximation [23,24], both of which are limited to the regime of sufficiently weak interactions. An alternative method is provided by the truncated Hamiltonian approach (THA), which can be used for stronger interactions [25].

THA was first invented to study relevant perturbations of minimal conformal field theories [26–28], later extended to

perturbations of other conformal field theories [29,30] and also to perturbations of the free massive fermion [31]. Truncated Hamiltonian methods suitable for φ^4 were developed in the works [32–36], including also for higher space-time dimensions [33]. An alternative approach to Hamiltonian truncation is provided by light-cone conformal truncation [37,38]. Truncated Hamiltonian methods proved efficient in simulating the full quantum out-of-equilibrium dynamics in $1+1$ dimensional quantum field theories [25,39–45]; for the case of perturbed conformal theories, an efficient algorithm including a MATLAB implementation was made publicly available recently [46].

In this paper, we apply the THA built upon a massive free boson basis [34–36] to study quantum quenches involving decay of the false vacuum the $1+1$ dimensional φ^4 theory, using the implementation developed in our previous work [25], and determine the tunneling rate per unit volume, which can be compared directly to theoretical predictions [47].

The outline of the paper is as follows. In Sec. II, we give a brief overview of the theory of the decay of the false vacuum. Section III introduces the formulation of false vacuum decay as a quantum quench, while Sec. IV specifies implementation of the nonequilibrium time evolution using the truncated Hamiltonian approach. The detailed results of our investigations are presented in Sec. V, while Sec. VI contains our conclusions.

II. DECAY OF THE FALSE VACUUM

Here, we briefly review the aspects of the decay of the false vacuum necessary for our investigations, including features specific for $1+1$ space-time dimensions. Following Coleman [1,2], false vacuum decays via bubble nucleation initiated by quantum fluctuations. The decay is dominated by spherically symmetric bubbles. Due to the finite energy of the walls (surface tension), bubbles smaller than a critical size only appear as short-lived quantum fluctuations. However, bubbles larger than a critical radius can form as stable field configurations, which then expand driven by the surplus vacuum energy density in the false vacuum compared to the true vacuum. In his seminal work [1], Coleman considered tunneling in a scalar field theory with a potential $U(\varphi)$, which has a global minimum corresponding to a stable ground state and a metastable local minimum corresponding to the false vacuum. In the semiclassical approximation, barrier penetration is described in terms of the instanton bounce φ_{I}, which is a spherically symmetric solution to the Euclidean equation of motion:

$$\left(\frac{\partial^2}{\partial\tau^2}+\nabla^2\right)\varphi=\frac{\partial U}{\partial\varphi}, \tag{1}$$

satisfying appropriate boundary conditions. The tunneling rate per unit volume V is then given by the formula,

$$\gamma=\frac{\Gamma}{V}=A\,\exp\left[-\frac{1}{\hbar}S_E\right], \tag{2}$$

where S_E is the Euclidean action of the instanton bounce, and the amplitude A can be expressed with the determinant of quantum fluctuations in the instanton background (note that it requires a careful treatment of zero modes).

The calculation simplifies considerably if the thickness of the walls is much smaller than the radius of the critical bubble, which is called the thin wall limit. The scalar potential is written as

$$U(\varphi)=U_0(\varphi)+\varepsilon\Delta U(\varphi), \tag{3}$$

where the term U_0 has two degenerate minima corresponding to vacua of equal energy density. The vacuum degeneracy is explicitly broken by switching on $\varepsilon>0$, and the thin wall limit corresponds to the limit of small ε [1]. In $1+1$ dimensions, the bubbles in the thin wall limit take the form of a kink-antikink pair delimiting a region with the true vacuum in its interior, and the diameter of the critical bubble is determined by simple energy conservation:

$$a_*=\frac{2M}{\mathcal{E}}, \tag{4}$$

where M is the kink mass, and $\mathcal{E}$ is the energy density difference between the false and true vacuum (latent heat):

$$\mathcal{E}=\frac{1}{L}(E_{\mathrm{FV}}-E_{\mathrm{TV}}). \tag{5}$$

In the thin wall limit, the action of a bubble with diameter a is

$$S(a)=\pi aM-\frac{\pi a^2}{4}\mathcal{E}, \tag{6}$$

which has its stationary point for $a=a_*$. As a result, nucleated bubbles are dominantly of the size a_*, and the instanton action determining the tunneling rate is

$$S_{\mathrm{E}}=\frac{\pi M^2}{\mathcal{E}}. \tag{7}$$

It is possible to go beyond the semiclassical limit to include quantum corrections [2]. Moreover, in $1+1$ dimensions, these were evaluated exactly in the thin wall limit by Voloshin [47] with the result,

$$\gamma=\frac{\mathcal{E}}{2\pi}\exp\left[-\frac{\pi M^2}{\mathcal{E}}\right], \tag{8}$$

where M is the exact renormalized kink mass, and $\mathcal{E}$ is the exact quantum energy density difference between the false and true vacua. Similar results were obtained for tunneling

in the quantum Ising spin chain [19] and were recently verified by numerical simulation of the spin chain dynamics [20].

III. VACUUM DECAY AS A QUANTUM QUENCH IN THE 1+1-DIMENSIONAL φ^4 THEORY

The action of φ^4 theory in the symmetry broken phase is given by

$$S[\varphi] = \int d^2x \left[\frac{1}{2}(\partial_t\varphi)^2 - \frac{1}{2}(\partial_x\varphi)^2 + \frac{m^2}{2}\varphi^2 - \frac{g}{6}\varphi^4 + \varepsilon\varphi\right], \tag{9}$$

which corresponds to setting,

$$U_0(\varphi) = -\frac{m^2}{2}\varphi^2 + \frac{g}{6}\varphi^4 \qquad \Delta U(\varphi) = -\varphi. \tag{10}$$

In the absence of explicit symmetry breaking (i.e., $\varepsilon = 0$), the classical ground states are

$$\varphi_\pm = \pm\sqrt{\frac{3m^2}{2g}}, \tag{11}$$

with kink/antikink excitation of mass,

$$M = \frac{\sqrt{2}m^3}{g}, \tag{12}$$

interpolating between them. Switching on a nonzero ε makes φ_+ the true ground state, while φ_- becomes the false vacuum (note that their positions are also slightly shifted).

At the quantum level, the two vacuum states and their characteristic parameters, such as the value of the order parameter and the vacuum energy density splitting, acquire quantum corrections, and the same is true for the kink mass M.

We investigate the false vacuum decay by setting up a quantum quench protocol. Denoting the quantum Hamiltonian of the $\varepsilon = 0$ theory with H, we initialize the system in the ground state $|\Psi_-\rangle$ of H, which becomes the false vacuum for $\varepsilon > 0$:

$$|\Psi(0)\rangle = |\Psi_-\rangle$$
$$H|\Psi_-\rangle = E_0|\Psi_-\rangle, \qquad \langle\Psi_-|\varphi|\Psi_-\rangle < 0. \tag{13}$$

At the initial time $t = 0$, we switch on $\varepsilon > 0$, and so the postquench Hamiltonian is

$$H_\varepsilon = H - \varepsilon\int dx\,\hat{\varphi}(x), \tag{14}$$

resulting in the unitary time evolution for $t > 0$:

$$|\Psi(t)\rangle = e^{-iH_\varepsilon t}|\Psi(0)\rangle. \tag{15}$$

The time evolution of an observable $\hat{\mathcal{O}}$ is given by the expectation value,

$$\langle\hat{\mathcal{O}}(t)\rangle \coloneqq \langle\Psi(t)|\hat{\mathcal{O}}|\Psi(t)\rangle. \tag{16}$$

We consider the time evolution of the order parameter, i.e., the expectation value of the field $\hat{\varphi}$, which we parametrize via the combination,

$$F(t) = \frac{\langle\hat{\varphi}(t)\rangle + \langle\hat{\varphi}(0)\rangle}{2\langle\hat{\varphi}(0)\rangle}, \tag{17}$$

inspired by the study of vacuum decay in the spin chain setting by Lagnese *et al.* [20]. Neglecting corrections of the vacuum expectation values of the field from the presence of the ε, the decay of the false vacuum corresponds to the change of $F(t)$ from 1 to 0, making it a convenient quantity to monitor the progression of the decay process.

IV. APPLYING THE TRUNCATED HAMILTONIAN APPROACH TO VACUUM DECAY

Now, we turn to the application of the truncated Hamiltonian approach to the time evolution starting from a false vacuum. The Hamiltonian can then be written as

$$H_\varepsilon = H^m_{\mathrm{KG}} + \int dx\,{:}\left(-m^2\hat{\varphi}^2 + \frac{g}{6}\hat{\varphi}^4 - \varepsilon\hat{\varphi}\right){:}_m, \tag{18}$$

where

$$H_{\mathrm{KG}} = \int dx\,{:}\left(\frac{1}{2}\hat{\pi}^2 + \frac{1}{2}(\partial_x\hat{\varphi})^2 + \frac{m^2}{2}\hat{\varphi}^2\right){:}_m \tag{19}$$

is the Klein-Gordon Hamiltonian of mass m, and the fields satisfy the equal time commutation relations,

$$[\hat{\pi}(t,x), \hat{\varphi}(t,x')] = -i\delta(x - x'), \tag{20}$$

while $:\ldots:_m$ denotes normal ordering with respect to the modes of the free Klein-Gordon field of mass m.

To implement the THA, we consider the system in a finite volume L with periodic (or antiperiodic) boundary conditions. Working in units $m = 1$, the system can be characterized by the following dimensionless parameters:

$$l = mL, \qquad \bar{g} = \frac{g}{m^2} \quad \text{and} \quad \bar{\varepsilon} = \frac{\varepsilon}{m^2}. \tag{21}$$

The finite volume Hamiltonian then takes the form,

$$H_{\mathrm{KG}}(L)=\int_0^L dx:\left(\frac{1}{2}\hat{\pi}^2+\frac{1}{2}(\partial_x\hat{\varphi})^2+\frac{m^2}{2}\hat{\varphi}^2\right):_{m,L}+E_0(L)$$
$$H_\varepsilon(L)=H^m_{\mathrm{KG}}+g_0(l)V_0+g_2(l)V_2+g_4(l)V_4-\varepsilon V_1$$
$$V_n=\int_0^l dx:\hat{\varphi}^n:_{m,L}. \tag{22}$$

Here, $:\ldots:_{m,L}$ denotes normal ordering with respect to the free bosonic modes with mass m in a finite volume L,

$$E_0(l)=\int_{-\infty}^{\infty}\frac{d\theta}{2\pi}\cosh\,\theta\,\log\,(1-e^{l\,\cosh\,\theta}), \tag{23}$$

and the finite volume couplings $g_i(l)$ are related to infinite volume couplings as [36]

$$g_0(l)=-m^2z^{\pm}(l)-m^2\frac{3\log 2}{8\pi}+\frac{g}{2}\tilde{z}^{\pm}(l)^2$$
$$g_2(l)=g\tilde{z}^{\pm}(l)-m^2\qquad g_4=\frac{g}{6}, \tag{24}$$

with

$$z^+(l)=\int_0^\infty\frac{d\theta}{\pi}\frac{1}{e^{l\,\cosh\,\theta}-1}\qquad z^-(l)=2z^+(2l)-z^+(l)$$
$$\tilde{z}^{\pm}(l)=z^{\pm}(l)+\frac{\log 2}{4\pi}, \tag{25}$$

where the $\pm$ superscript refers to (anti)periodic boundary conditions $\hat{\varphi}(x+L)=\pm\hat{\varphi}(x)$.

The next step is to separate the zero mode using the "minisuperspace" method [35,36] to take into account the main effect of symmetry breaking (including the tunneling), which highly improves the convergence of the method. Writing

$$\hat{\varphi}(x)=\hat{\varphi}_0+\tilde{\varphi}(x),\qquad \hat{\varphi}_0=\frac{1}{L}\int_0^L dx\hat{\varphi}(x), \tag{26}$$

where $\hat{\varphi}_0$ is the zero mode, while $\tilde{\varphi}(x)$ is the nonzero mode of the field, and separating the Hilbert space accordingly as

$$\mathcal{H}=\mathcal{H}^{\mathrm{mini}}\otimes\tilde{\mathcal{H}}, \tag{27}$$

the Hamiltonian can be decomposed as

$$H_\varepsilon=\tilde{H}^m_{\mathrm{KG}}+H^{\mathrm{mini}}_\varepsilon+\int_0^L dx[g_0+g_2:\tilde{\varphi}(x)^2:$$
$$+g_4(:\tilde{\varphi}(x)^4:+6:\tilde{\varphi}(x)^2:\hat{\varphi}_0^2+4:\tilde{\varphi}(x)^3:\hat{\varphi}_0)]$$
$$H^{\mathrm{mini}}_\varepsilon=L\left[\frac{1}{2}:\hat{\pi}_0^2:+\frac{m^2}{2}:\hat{\varphi}_0^2:+g_2:\hat{\varphi}_0^2:+g_4:\hat{\varphi}_0^4:\right.$$
$$\left.-\varepsilon:\hat{\varphi}_0:\right], \tag{28}$$

where $\hat{\pi}_0$ is the zero mode conjugate momentum, and $\tilde{H}^m_{\mathrm{KG}}$ denotes the free Klein-Gordon Hamiltonian with the zero mode omitted. We note that this step is only necessary for periodic boundary conditions since there is no zero mode in the antiperiodic case.

Representing the Hamiltonian on the Fock space of the Klein-Gordon model with mass m in finite volume L with (anti)periodic boundary conditions, its matrix elements can be explicitly evaluated. The space decomposes in sectors of different total momentum; in our subsequent computations, we only need the sector with zero total momentum.

The space is made finite dimensional by introducing an ultraviolet (UV) cutoff separately in the minisuperspace and the space of nonzero modes. In the minisuperspace $\mathcal{H}^{\mathrm{mini}}$, the procedure is to diagonalize numerically the zero mode Hamiltonian and keep a suitably large number of the lowest lying eigenstates; we chose a cutoff for this numerical diagonalization such that the energy levels kept after this diagonalization can be considered numerically exact. For the nonzero modes, we impose an upper energy cutoff Λ in the total energy computed with the KG part of the Hamiltonian. The cutoff Λ is parametrized as

$$\frac{\Lambda}{m}=\frac{4\pi n_{\max}}{l}, \tag{29}$$

where $n_{\max}$ is a dimensionless parameter, which can be interpreted as to the maximum momentum quantum number that is allowed to be filled when neglecting m.

The spectrum of the Hamiltonian obtained in this way still depends on the UV cutoff. The leading order dependence on the nonzero mode cutoff Λ can be eliminated by a renormalization of the Hamiltonian [35]:

$$H^{\mathrm{RG}}_\varepsilon=H_\varepsilon+\int_0^L dx[\kappa_0+\kappa_2:\tilde{\varphi}(x)^2:$$
$$+\kappa_4(:\tilde{\varphi}(x)^4:+6:\tilde{\varphi}(x)^2:\varphi_0^2+4:\tilde{\varphi}(x)^3:\varphi_0)], \tag{30}$$

where explicit expressions for the κ_n are given in the literature [25,35]. The zero-mode part, however, can be considered essentially exact; the only condition is to keep sufficient number of states to be consistent with the nonzero mode cutoff Λ.

V. RESULTS

To evaluate (8), it is necessary to know the values of the kink mass and of the latent heat.

A. Kink mass

The kink mass can be computed by setting $\bar{\varepsilon}=0$ and computing the difference between the lowest levels in the antiperiodic and periodic sectors, which correspond to a stationary kink and the vacuum state, respectively. Note that for antiperiodic boundary conditions, there are no zero

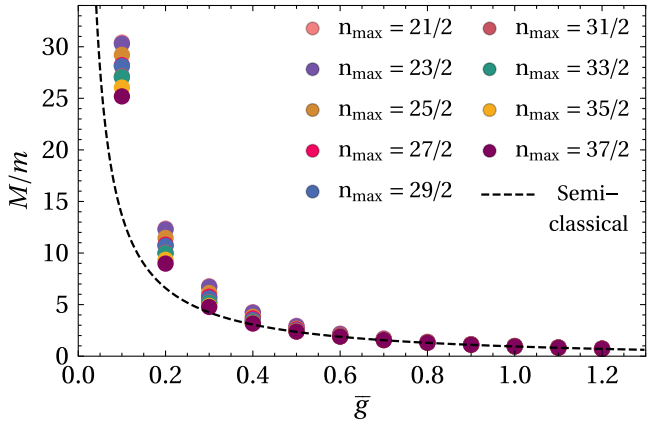

FIG. 1. The kink masses as obtained via THA (markers) together with the semiclassical prediction. The different colors denote different values of the cutoff $n_{max} = 21/2, \ldots 37/2$ corresponding to cc. 1000–100000 basis states.

modes, so the procedure outlined above simplifies. Figure 1 shows the g-dependence of the kink mass [36] for various values of the cutoff n_{max} together with the semiclassical prediction [48],

$$M = \frac{\sqrt{2}m^3}{g} - \sqrt{2}m\left(\frac{3}{2\pi} - \frac{1}{4\sqrt{3}}\right) + O(g). \quad (31)$$

Note that for small couplings, the kink mass is large, and therefore, it has a strong dependence on the UV cutoff, while for larger couplings, the kink masses agree very well with the semiclassical prediction.

B. Latent heat

The latent heat $\mathcal{E}$ is the difference of energy density between the true and false vacuum, which can be easily

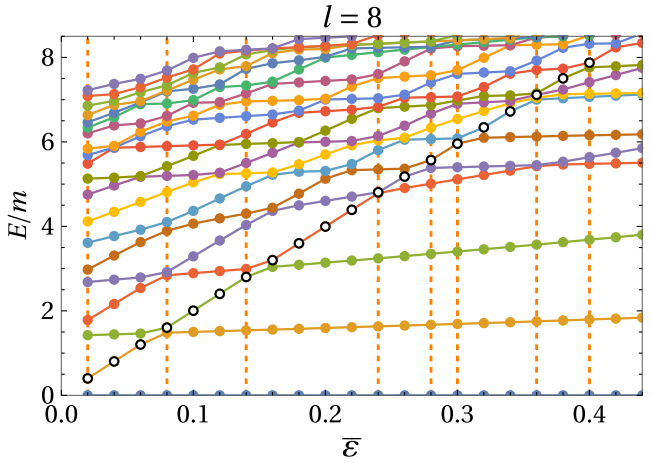

FIG. 2. The spectrum of H_ε for $l = 8$ and $\bar{g} = 1.1$ as a representative spectrum of the asymmetric theory, with the true vacuum line subtracted. The false vacuum line is denoted by open black markers.

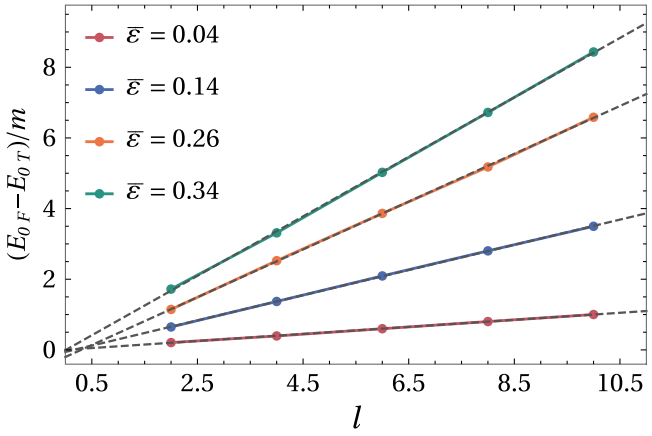

FIG. 3. The energy difference between the false and true vacuum as a function of the volume with the linear dependence fitted for some values of the symmetry breaking field ε for $\bar{g} = 1.1$. The slope of the fitted linear curve is the energy density difference (latent heat) $\mathcal{E}$ for a given $\bar{\varepsilon}$.

computed from the THA diagonalizing H_ε by considering the spectrum as a function of $\bar{\varepsilon}$ for fixed volumes as illustrated in Fig. (2) for $\bar{g} = 1.1$ and $l = 8$. Performing this procedure for several values of the volume, we can then plot the vacuum energy splitting as a function of the volume for each value of the symmetry breaking parameter ε, which is shown in Fig. 3 for $\bar{g} = 1.1$. The slope of these lines gives the value of the latent heat $\mathcal{E}(\bar{\varepsilon})$ as a function of $\bar{\varepsilon}$. For small ε, this function is expected to be linear corresponding to first order in perturbation theory, which turns out to hold in all the range of ε needed for the later computations of the vacuum decay as shown in Fig. 4 for various values of $\bar{g}$. As a result, the latent heat can be parametrized by fitting a linear relation,

$$\mathcal{E} = A(\bar{g})\bar{\varepsilon}, \quad (32)$$

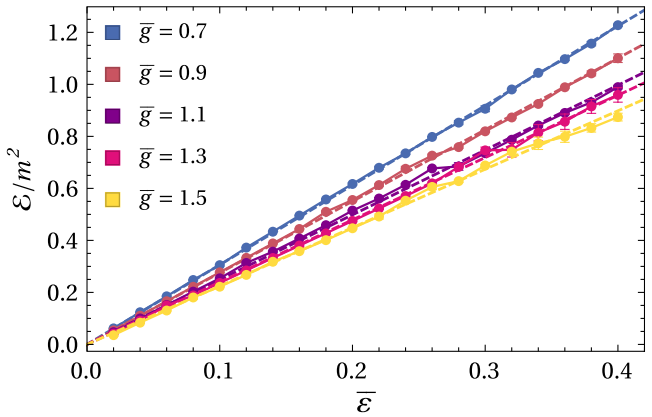

FIG. 4. The latent heat $\mathcal{E}$ as a function of $\bar{\varepsilon}$ for various couplings $\bar{g}$ with the fitted linear dependence. The error bars represent a crude estimate obtained from the uncertainty of the parameter estimation from the fits shown in Fig. 3.

and extracting the coefficient $A(\bar{g})$, which only depends on $\bar{g}$. The procedure was carried out for several different values of $\bar{g}$, with a nonzero mode basis of around 1000 states and a minisuperspace dimension of 11, which provided sufficient accuracy as demonstrated by the results presented in the plots.

C. Bubble nucleation rate

Having computed the kink mass and the latent heat in the quantum theory, we turn to the evaluation of the tunneling rate via the THA using the quantum quench setting presented in Sec. III. The tunneling rate is computed as a function of the latent heat $\mathcal{E}$, which is controlled using the symmetry breaking parameter $\bar{\varepsilon}$. The validity of the THA simulation restricts the range of $\bar{\varepsilon}$ for which the simulation makes sense:

(i) To avoid finite size effects, the size of the critical bubble [Eq. (4)] must be smaller than the volume L, at least by a few times the correlation length (which, for the regime of coupling considered here, is of order $1/m$).

(ii) The false vacuum state must fit below the cutoff; therefore, it is necessary to fulfil $\mathcal{E} = A(\bar{g})\bar{\varepsilon} \ll \Lambda$.

These two conditions impose a lower and upper limit on the values of $\bar{\varepsilon}$ for the simulations, which depend on the self-interaction $\bar{g}$. We simulated the time evolution in a volume $l = 20$, using a minisuperspace dimension of 41 and verified that the results were stable against increasing the number of zero-mode eigenstates kept. For the nonzero modes, the cutoff was varied with the values $n_{\max} = 10$, 12, 14, 16, and 18, with the dimension of the truncated Hilbert space going up to cc. 280000. With these parameters and settings, it was possible to estimate the available interval for $\bar{\varepsilon}$ at any fixed choice for $\bar{g}$. Finally, we chose values for $\bar{g}$ for which this interval was large enough so that the dependence of the decay rate on $\bar{\varepsilon}$ could be seen in a reasonable interval.

Figure 5 shows the time evolution of $F(t)$ for coupling $\bar{g} = 1.1$ and different values of the symmetry breaking field $\bar{\varepsilon}$. For small values $\bar{\varepsilon}$, the size [Eq. (4)] of the resonant bubble is too large compared to the volume, preventing nucleation and leading instead to persistent oscillations. For larger $\bar{\varepsilon}$, the nature of the time evolution changes: After a short initial transient corresponding to quantum Zeno regime [49,50] where the time dependence is quadratic, a time window with exponential decay of $F(t)$ follows, which can be more easily identified as a linear drop on the plot of log $F(t)$ shown in Fig. 6. The validity of exponential behavior is limited in time, however, and it is followed by oscillations with their amplitude apparently decreasing in time with a power law, although the available time window is not a long enough time to make this observation more precise. Note that even if the oscillating regime were absent, the range of time evolution available in the THA is limited from above by the volume, since for $t > L$, excitations can travel around the circle, resulting in deviations from infinite volume behavior. Therefore, the exponential behavior can only be observed in a finite time window. We return to a more detailed discussion of the theoretical and methodological limitations of simulating the vacuum decay in the conclusions.

To determine the tunneling rate, we plot the logarithm of $F(t)$ and determine the slope of the linear segment in the logarithmic plot. This was carried out for various quartic couplings $\bar{g}$ and $\bar{\varepsilon}$, with some representative plots shown in Fig. 6 corresponding to $\bar{g} = 1.1$ and $l = 20$. Identification of the linear segment is simpler for larger values of $\bar{\varepsilon}$, while for smaller $\bar{\varepsilon}$, the identification is helped by following the

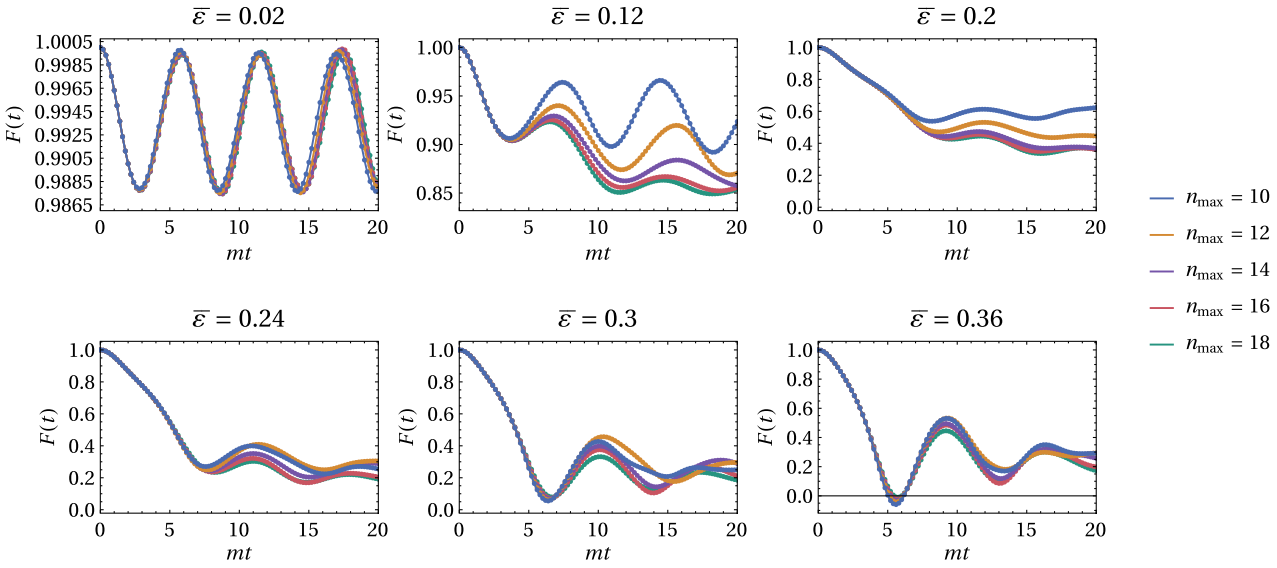

FIG. 5. Time evolution of $F(t)$ for $\bar{g} = 1.1$ and different values of ε. The different colors denote different values of the cutoff. Here, results corresponding to $n_{\max} = 10$, 12, 14, 16, and 18 are presented, corresponding to cc. 4100–287000 states.

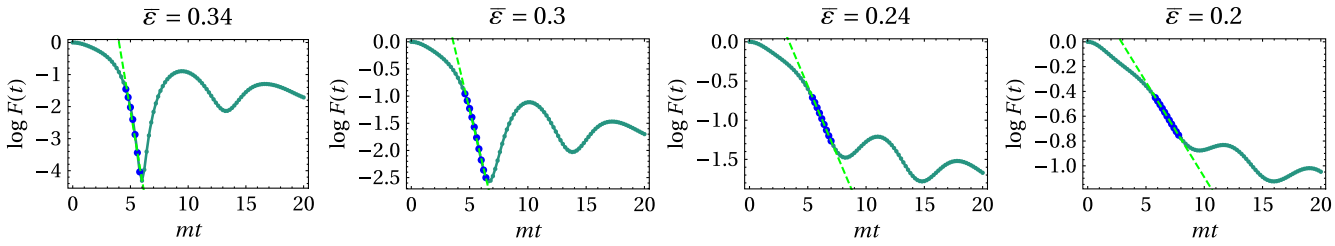

FIG. 6. The logarithm of $F(t)$ for $l = 20$ and $\bar{g} = 1.1$ obtained with the largest cutoff $n_{\max} = 18$, plotted together with the linear fits to the apparent tunneling regime. The slope of the linear fits gives the tunneling rate Γ.

time evolution gradually from larger to smaller values of the symmetry breaking field. Dividing by the value of L gives the nucleation rate per unit volume, which is shown in Fig. 7 for $l = 20$, and various couplings as discrete data points connected by continuous lines for convenience. The dashed curves show the theoretical prediction computed using the kink mass M and latent heat $\mathcal{E}$ extracted from THA using the formula,

$$\gamma = C(\bar{g})\frac{\mathcal{E}}{2\pi}\exp\left[-\frac{\pi M^2}{\mathcal{E}}\right], \tag{33}$$

which differs from Voloshin's result (8) by including a $\bar{g}$-dependent factor $C(\bar{g})$, which is a fitting parameter that can be used to translate the prediction curve to overlay it with the simulation results. Note that apart from this factor, the $\bar{\varepsilon}$ dependence follows the theoretical prediction very well. The appearance of such a redefinition is eventually expected since the same proved necessary when comparing

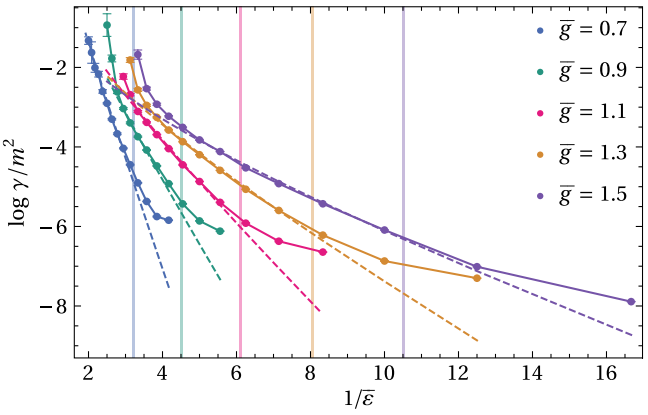

FIG. 7. The logarithm of γ obtained from THA (with $n_{\max} = 18$) for various couplings in $l = 20$ as a function of $1/\bar{\varepsilon}$ together with the theoretical predictions (8) (dashed lines). The vertical lines correspond to the values of the symmetry breaking field values where the resonant bubble size reaches $a_* = l/2$, demonstrating that the difference between the theoretical and numerical results for small values of $\bar{\varepsilon}$ originate from finite size effects. The error bars represent a crude estimate obtained from the uncertainty of the parameter estimation from the fits, a representative sample of which is shown in Fig. 6.

simulation results for the transverse field Ising spin chain [20] with the corresponding theoretical predictions [19].

The match between the numerical and theoretical results is made stronger by observing that it holds for different values of the coupling strength $\bar{g}$. In all cases, the curves show deviations both for small and for large values of $\bar{\varepsilon}$. For small values of $\bar{\varepsilon}$ (i.e., large values of $1/\bar{\varepsilon}$), the disagreement originates from finite size effects resulting from the size of the resonant bubble (4) being comparable to the volume. The color-coded vertical lines in Fig. 7 are drawn at values of $\bar{\varepsilon}$ where the resonant bubble size a_* is equal to half the volume. It can be clearly seen that this coincides well with the regime where the numerical results start to deviate appreciably from the theoretical predictions.

The deviations for large values of the symmetry breaking field the numerical data can have two different origins. First, the theoretical predictions assume the thin wall approximation, which assumes a suitable small value of the symmetry breaking field, although we cannot really provide a concrete estimate for the value where the prediction should fail. In addition, for larger values of the latent heat, the energy injected by the quantum quench becomes comparable with the truncation, leading to loss of precision of the numerical simulation. In addition, large values of the symmetry breaking field $\bar{\varepsilon}$ can even lead to the disappearance of the local minimum corresponding to the false vacuum, changing the dynamics entirely.

To test whether the factor $C(\bar{g})$ depends on the volume, we carried out simulations in other volumes $l = 25$ and 30. For these simulations, we used a minisuperspace of dimension of 41, together with a nonzero mode cutoff of $n_{\max} = 18$, 22, and 24, resulting in Hilbert space dimensions of cc. 280000, 680000, and 680000 for $l = 20$, 25, and 30, respectively. As illustrated in Fig. 8, the results show that $\log C(\bar{g})$ (which is the quantity directly obtained) shows no dependence on the volume. For large $1/\bar{\varepsilon}$, where the limiting factor is the finite system size, the agreement between the simulations and the prediction (33) improves with larger volume, as expected. The deviations for small $1/\bar{\varepsilon}$ grow with the volume, which suggests that rather than resulting from the invalidity of the thin wall approximation, this discrepancy is caused by truncation effects since, according to (29), the physical cutoff Λ in units of m is

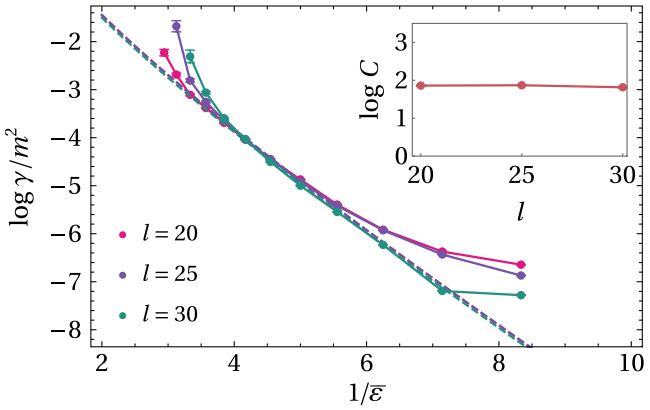

FIG. 8. The (logarithm of the) nucleation rate γ obtained from THA for different volumes l at interaction $\bar{g} = 1.1$ as a function of $1/\bar{\varepsilon}$ together with the theoretical predictions (33). The inset shows the fitted values of $\log C$ for different values of the volume, where the (barely visible) error bars show the uncertainty of the parameter estimation from the fits.

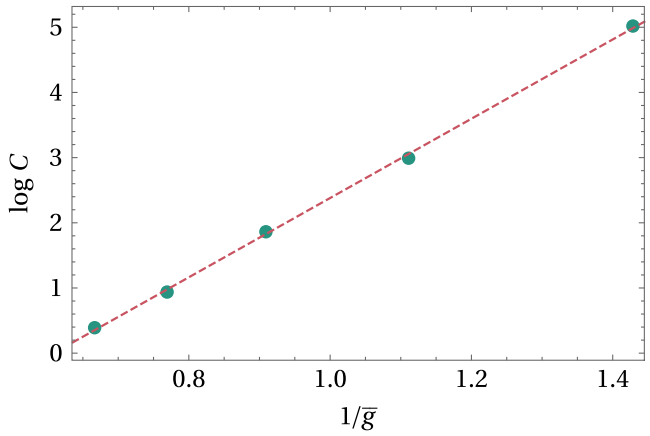

FIG. 9. THA results (with $n_{\max} = 18$) for the logarithm of the prefactor C plotted as a function of the inverse of the interaction strength $1/\bar{g}$ together with a linear fit. The numerical evaluation was performed in volume $l = 20$.

$4\pi n_{\max}/l$, which, in our simulations, was decreasing with the volume.

Figure 9 shows the numerically obtained values of $\log C$ as a function of $1/\bar{g}$, extracted in volume $l = 20$ as in Fig. 7, which suggests that the correct prefactor in the nucleation rate has a highly nonperturbative dependence on the interaction strength.

VI. CONCLUSIONS

We investigated the decay of the false vacuum in the $1 + 1$ dimensional φ^4 theory by studying the time evolution of the order parameter triggered by a quantum quench. We simulated the dynamics by a truncated Hamiltonian approach built using the Fock space of the free massive boson as computational basis and demonstrated the existence of a regime of exponential decay and extracted its rate. The decay rate normalized to unit volume was first computed theoretically in the semiclassical approximation by Coleman [1,2]; here, we used a later prediction by Voloshin [47], which is expected to be exact at the quantum level if the nucleated bubbles are in the thin wall limit. Apart from an overall normalization factor $C(\bar{g})$, we found that the numerically determined decay rate considered as a function of the latent heat matches the theoretical predictions well. The appearance of $C(\bar{g})$ is consistent with recent results obtained in the spin chain setting [20]. Beyond the overall prefactor, the observed deviations are consistent with the expected limitations of the theoretical approach and the numerical simulation.

Extracting the nucleation rate from the decay rate of the order parameter is subject to certain general, as well as method specific limitations. Concerning the general limitations, at short times, the exponential behavior is absent due to general principles of quantum theory, while for later times, a complicated dynamics takes place involving the expansion and collision of nucleated bubbles, and finally, thermalization of the resulting finite density medium [20]. Specifically for the THA method, our results demonstrate that despite that the available time window is limited by the finite volume, it can still access the full time range in which the exponential behavior holds.

As already mentioned in the Introduction, the decay of the false vacuum was recently studied in quantum spin chains using tensor network methods [20], for which time evolution can be simulated directly in infinite volume using tensor network methods, which is a definite advantage over the THA. However, in spite of the absence of finite size effects, tensor network methods are still limited in their time range due to the buildup of entanglement. In addition, time evolution in spin chains is affected by lattice effects such as, e.g., Bloch oscillations [51], that can prevent the subsequent expansion, and therefore thermalization, of the nucleated bubbles [21], while from the point of view of field theory, the truncated Hamiltonian approach has the advantage that lattice effects are absent.

Now we turn to the issue of the appearance of the fitting parameter $C(\bar{g})$. The predicted nucleation rate (8) has the form,

$$\gamma = \frac{\mathcal{E}}{2\pi} \exp\left[-\frac{\pi M^2}{\mathcal{E}}\right], \tag{34}$$

consisting of the exponential of the instanton action and a prefactor resulting from quantum fluctuations. The observed rate (33) agrees with the above prediction if $C(\bar{g})$ is set to 1. In our comparison, we eventually looked at the logarithm of the rate, whose dependence on the latent heat is dominated by the $1/\mathcal{E}$ coming from the instanton action; the presence and also the precise value of this

contribution are strongly confirmed by the comparison to the simulation results. The fluctuations contribute a dependence $\log \mathcal{E}$ to $\log \gamma$, and while its presence is consistent with our simulation results, it cannot be verified to high precision due to the slowly changing nature of the logarithm. Nevertheless, the observed agreement strongly suggests that the relative factor $C(\bar{g})$ between the theoretical predictions and numerical results is independent of the latent heat $\mathcal{E}$ as well as the volume L. The numerical data also indicate that $\log C(\bar{g})$ is inversely proportional to the interaction strength $\bar{g}$. The precise origin of the factor $C(\bar{g})$ is not clear to us at present and deserves further investigation.

Other interesting avenues to explore is to extend our studies beyond the thin wall regime and also to other $1 + 1$ dimensional quantum field theories. In addition, the late time behavior eventually corresponds to thermalization dynamics, which is another interesting physical regime to study in the future.

ACKNOWLEDGMENTS

This work was supported by the National Research, Development and Innovation Office (NKFIH) through the OTKA Grants K 138606, and also within the Quantum Information National Laboratory of Hungary.

[1] S. Coleman, Fate of the false vacuum: Semiclassical theory, Phys. Rev. D **15**, 2929 (1977).
[2] C. G. Callan, Jr. and S. Coleman, Fate of the false vacuum. II. First quantum corrections, Phys. Rev. D **16**, 1762 (1977).
[3] J. Elias-Miró, J. R. Espinosa, G. F. Giudice, G. Isidori, A. Riotto, and A. Strumia, Higgs mass implications on the stability of the electroweak vacuum, Phys. Lett. B **709**, 222 (2012).
[4] T. P. Billam, R. Gregory, F. Michel, and I. G. Moss, Simulating seeded vacuum decay in a cold atom system, Phys. Rev. D **100**, 065016 (2019).
[5] T. P. Billam, K. Brown, and I. G. Moss, Simulating cosmological supercooling with a cold atom system, Phys. Rev. A **102**, 043324 (2020).
[6] K. Lun Ng, B. Opanchuk, M. Thenabadu, M. Reid, and P. D. Drummond, The fate of the false vacuum: Finite temperature, entropy and topological phase in quantum simulations of the early universe, PRX Quantum **2**, 010350 (2021).
[7] T. P. Billam, K. Brown, A. J. Groszek, and I. G. Moss, Simulating cosmological supercooling with a cold atom system II, arXiv:2104.07428.
[8] S. Abel and M. Spannowsky, Observing the fate of the false vacuum with a quantum laboratory, PRX Quantum **2**, 010349 (2021).
[9] S. Hofferberth, I. Lesanovsky, B. Fischer, T. Schumm, and J. Schmiedmayer, nonequilibrium coherence dynamics in one-dimensional Bose gases, Nature (London) **449**, 324 (2007).
[10] S. Trotzky, Y. A. Chen, A. Flesch, I. P. McCulloch, U. Schollwöck, J. Eisert, and I. Bloch, Probing the relaxation towards equilibrium in an isolated strongly correlated one-dimensional Bose gas, Nat. Phys. **8**, 325 (2012).
[11] M. Gring, M. Kuhnert, T. Langen, T. Kitagawa, B. Rauer, M. Schreitl, I. Mazets, D. A. Smith, E. Demler, and J. Schmiedmayer, Relaxation and prethermalization in an isolated quantum system, Science **337**, 1318 (2012).
[12] M. Cheneau, P. Barmettler, D. Poletti, M. Endres, P. Schauß, T. Fukuhara, C. Gross, I. Bloch, C. Kollath, and S. Kuhr, Light-cone-like spreading of correlations in a quantum many-body system, Nature (London) **481**, 484 (2012).
[13] F. Meinert, M. J. Mark, E. Kirilov, K. Lauber, P. Weinmann, A. J. Daley, and H. C. Nägerl, Quantum Quench in an Atomic One-Dimensional Ising Chain, Phys. Rev. Lett. **111**, 053003 (2013).
[14] T. Langen, R. Geiger, M. Kuhnert, B. Rauer, and J. Schmiedmayer, Local emergence of thermal correlations in an isolated quantum many-body system, Nat. Phys. **9**, 640 (2013).
[15] T. Fukuhara, P. Schauß, M. Endres, S. Hild, M. Cheneau, I. Bloch, and C. Gross, Microscopic observation of magnon bound states and their dynamics, Nature (London) **502**, 76 (2013).
[16] A. M. Kaufman, M. E. Tai, A. Lukin, M. Rispoli, R. Schittko, P. M. Preiss, and M. Greiner, Quantum thermalization through entanglement in an isolated many-body system, Science **353**, 794 (2016).
[17] P. Calabrese and J. L. Cardy, Time-Dependence of Correlation Functions Following a Quantum Quench, Phys. Rev. Lett. **96**, 136801 (2006).
[18] P. Calabrese and J. Cardy, Quantum quenches in extended systems, J. Stat. Mech. (2007) P06008.
[19] S. B. Rutkevich, Decay of the metastable phase in $d = 1$ and $d = 2$ Ising models, Phys. Rev. B **60**, 14525 (1999).
[20] G. Lagnese, F. M. Surace, M. Kormos, and P. Calabrese, False vacuum decay in quantum spin chains, Phys. Rev. B **104**, L201106 (2021).
[21] O. Pomponio, M. A. Werner, G. Zaránd, and G. Takacs, Bloch oscillations and the lack of the decay of the false vacuum in a one-dimensional quantum spin chain, SciPost Phys. **12**, 061 (2022).
[22] S. Sotiriadis and J. Cardy, Quantum quench in interacting field theory: A self-consistent approximation, Phys. Rev. B **81**, 134305 (2010).
[23] A. Polkovnikov, Quantum corrections to the dynamics of interacting bosons: Beyond the truncated Wigner approximation, Phys. Rev. A **68**, 053604 (2003).

[24] A. Polkovnikov, Phase space representation of quantum dynamics, Ann. Phys. (Amsterdam) **325**, 1790 (2010).
[25] D. Szász-Schagrin, I. Lovas, and G. Takács, Quantum quenches in an interacting field theory: Full quantum evolution versus semiclassical approximations, Phys. Rev. B **105**, 014305 (2022).
[26] V. Yurov and A. Zamolodchikov, Truncated conformal space approach to scaling Lee-Yang model, Int. J. Mod. Phys. A **05**, 3221 (1990).
[27] V. P. Yurov and A. B. Zamolodchikov, Truncated-fermionic approach to the critical 2d Ising model with magnetic field, Int. J. Mod. Phys. A **06**, 4557 (1991).
[28] M. Lässig and G. Mussardo, Hilbert space and structure constants of descendant fields in two-dimensional conformal theories, Comput. Phys. Commun. **66**, 71 (1991).
[29] G. Feverati, F. Ravanini, and G. Takács, Truncated conformal space at $c = 1$, nonlinear integral equation and quantization rules for multi-soliton states, Phys. Lett. B **430**, 264 (1998).
[30] R. M. Konik, T. Pálmai, G. Takács, and A. M. Tsvelik, Studying the perturbed Wess-Zumino-Novikov-Witten SU $(2)_k$ theory using the truncated conformal spectrum approach, Nucl. Phys. **B899**, 547 (2015).
[31] P. Fonseca and A. Zamolodchikov, Ising field theory in a magnetic field: Analytic properties of the free energy, arXiv:hep-th/0112167.
[32] A. Coser, M. Beria, G. P. Brandino, R. M. Konik, and G. Mussardo, Truncated conformal space approach for 2D Landau-Ginzburg theories, J. Stat. Mech. (2014) P12010.
[33] M. Hogervorst, S. Rychkov, and B. C. van Rees, Truncated conformal space approach in d dimensions: A cheap alternative to lattice field theory?, Phys. Rev. D **91**, 025005 (2015).
[34] S. Rychkov and L. G. Vitale, Hamiltonian truncation study of the φ^4 theory in two dimensions, Phys. Rev. D **91**, 085011 (2015).
[35] S. Rychkov and L. G. Vitale, Hamiltonian truncation study of the ϕ^4 theory in two dimensions. II. The Z_2 -broken phase and the Chang duality, Phys. Rev. D **93**, 065014 (2016).
[36] Z. Bajnok and M. Lájer, Truncated Hilbert space approach to the 2d ϕ^4 theory, J. High Energy Phys. 10 (2016) 050.
[37] E. Katz, Z. U. Khandker, and M. T. Walters, A conformal truncation framework for infinite-volume dynamics, J. High Energy Phys. 07 (2016) 140.
[38] N. Anand, A. L. Fitzpatrick, E. Katz, Z. U. Khandker, M. T. Walters, and Y. Xin, Introduction to lightcone conformal truncation: QFT dynamics from CFT data, arXiv:2005.13544.
[39] T. Rakovszky, M. Mestyán, M. Collura, M. Kormos, and G. Takács, Hamiltonian truncation approach to quenches in the Ising field theory, Nucl. Phys. **B911**, 805 (2016).
[40] D. X. Horváth and G. Takács, Overlaps after quantum quenches in the sine-Gordon model, Phys. Lett. B **771**, 539 (2017).
[41] K. Hódsági, M. Kormos, and G. Takács, Quench dynamics of the Ising field theory in a magnetic field, SciPost Phys. **5**, 027 (2018).
[42] I. Kukuljan, S. Sotiriadis, and G. Takács, Correlation Functions of the Quantum Sine-Gordon Model in and out of Equilibrium, Phys. Rev. Lett. **121**, 110402 (2018).
[43] K. Hódsági, M. Kormos, and G. Takács, Perturbative postquench overlaps in quantum field theory, J. High Energy Phys. 08 (2019) 047.
[44] D. X. Horváth, I. Lovas, M. Kormos, G. Takács, and G. Zaránd, Nonequilibrium time evolution and rephasing in the quantum sine-Gordon model, Phys. Rev. A **100**, 013613 (2019).
[45] I. Kukuljan, Continuum approach to real time dynamics of $(1 + 1)$D gauge field theory: Out of horizon correlations of the Schwinger model, Phys. Rev. D **104**, L021702 (2021).
[46] D. X. Horváth, K. Hódsági, and G. Takács, Chirally factorised truncated conformal space approach, Comput. Phys. Commun. **277**, 108376 (2022).
[47] M. B. Voloshin, Decay of false vacuum in $(1 + 1)$ dimensions, Report No. ITEP-8(1985), Institute of Theoretical and Experimental Physics, Moscow, Russia, 1985, https://inis.iaea.org/search/17020133.
[48] R. F. Dashen, B. Hasslacher, and A. Neveu, Nonperturbative methods and extended-hadron models in field theory. II. Two-dimensional models and extended hadrons, Phys. Rev. D **10**, 4130 (1974).
[49] A. Degasperis, L. Fonda, and G. C. Ghirardi, Does the lifetime of an unstable system depend on the measuring apparatus?, Nuovo Cimento A **21**, 471 (1974).
[50] B. Misra and E. C. G. Sudarshan, The Zeno's paradox in quantum theory, J. Math. Phys. (N.Y.) **18**, 756 (1977).
[51] A. Lerose, F. M. Surace, P. P. Mazza, G. Perfetto, M. Collura, and A. Gambassi, Quasilocalized dynamics from confinement of quantum excitations, Phys. Rev. B **102**, 041118(R) (2020).